Microwave excitations associated with a wavy angular dependence of the spin transfer torque: Model and experiments

O. Boulle,* V. Cros,† J. Grollier, L. G. Pereira,‡ C. Deranlot, and F. Petroff
Unité Mixte de Physique CNRS/Thales and Université Paris Sud 11, Route Départementale 128, 91767 Palaiseau, France

G. Faini
Phynano Team, Laboratoire de Photonique et de Nanostructures LPN-CNRS, Route de Nozay, 91460 Marcoussis, France

J. Barnaś
Department of Physics, Adam Mickiewicz University, Umultowska 85, 61-614 Poznan, Poland

A. Fert
Unité Mixte de Physique CNRS/Thales and Université Paris Sud-11, Route Départementale 128, 91767 Palaiseau, France
(Received 4 December 2007; published 2 May 2008)

The spin transfer torque (STT) can lead to a steady precession of magnetization without any external applied field in magnetic spin valves where the magnetic layers have very different spin diffusion lengths. This effect is associated with a nonstandard dependence of the STT, called "wavy" angular dependence of the STT (WAD-STT), predicted in the frame of diffusive models of spin transfer. In this paper, we present a complete experimental characterization of the magnetization dynamics in the presence of a WAD-STT. The results are compared to the prediction of the magnetization dynamics obtained by single domain magnetic simulations (macrospin approximation). The macrospin simulations reproduce well the main static and dynamical experimental features and suggest that the dynamical excitations experimentally observed are associated with a large angle out-of-plane precession mode. The present work validates the diffusive models of the spin transfer and underlines the role of the spin accumulation and the spin relaxation effects on the STT.

DOI: 10.1103/PhysRevB.77.174403 PACS number(s): 85.75.−d, 75.47.−m, 75.40.Gb

I. INTRODUCTION

A spin polarized current can exert a torque on the magnetization of a ferromagnetic body via the transfer of a spin angular momentum. This spin transfer effect, which was introduced originally by Slonczewski[1] and Berger,[2] has opened a new route for the manipulation of a magnetization using an electrical current. In most experiments, it has been studied in a pillar shaped F1/NM/F2 trilayer, in which a magnetic layer F1 with a fixed magnetization is used to prepare a spin polarized current injected in a magnetically free magnetic layer F2. When the spin polarized current enters the free layer, the part of the spin current that is transverse to the magnetization is absorbed and transferred to the local magnetization; this spin transfer is equivalent to a torque exerted on magnetization. In *standard* structures such as Co/Cu/Co at zero or low applied field, the spin transfer torque (STT) leads to an irreversible switching of the magnetization from one static configuration to another.[3,4] For larger fields (typically higher than the coercive field), the spin transfer torque compensates for the damping torque, resulting in a steady precession of magnetization. The giant magnetoresistance (GMR) effect converts this high frequency precession into voltage oscillations in the microwave range.[5,6] These two behaviors (magnetization switching and precession) open two branches of potential technological applications of the spin transfer effect: First, a more reliable way to write the magnetic bit in magnetic memories, and second, a new type of submicrometric microwave oscillators for telecommunication devices combining a high quality factor and a large frequency agility with current and field.[6]

Following the original approach of Slonczewski,[1] several theoretical studies underlined that the STT is directly related to the polarization of the spin current entering the magnetic free layer and more precisely to the absorption of the component of the spin current that is transverse to the magnetization.[7,8] In the first spin transfer models,[1,9] the magnetic multilayer was contacted to reservoirs with uniform chemical potentials and the spin polarization arose from the spin dependent reflections at the interfaces of the multilayer. However, since the study of the GMR effect in the geometry where the current is flowing perpendicularly to the plane of the layers (CPP-GMR),[10,11] it has become well known that the spin polarization of the current is strongly affected by the spin dependent scattering inside the magnetic layers as well as the spin relaxation effects. Indeed, recent spin transfer models do take into account these diffusive transport aspects.[8,12–19]

The first experimental evidence of the influence of the diffusive transport aspects on the STT was given by Urazhdin *et al.*[20] and AlHajDarwish *et al.*[21] They demonstrated the influence of the *spin dependent scattering* by magnetic impurities on the STT in the low field switching regime: By doping the polarizing layer with impurities, the amplitude and even the sign of the torque were changed. More recently, we experimentally demonstrated the influence of the *spin relaxation effect* on the STT.[22] We studied the magnetization dynamics induced by the STT in a Co (8 nm)/Cu/Py (8 nm) ($Py=Ni_{80}Fe_{20}$) nanopillar, in which a nonstandard angular dependence of the STT on the angle φ between both magnetizations is predicted in the frame of diffusive models of spin

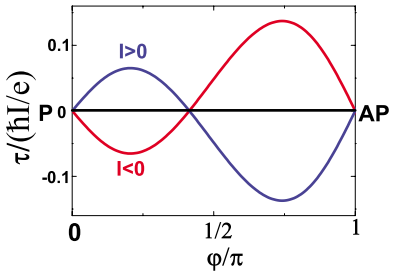

FIG. 1. (Color online) Magnitude of the spin transfer torque τ on the free Py layer of a Au (infinite)/Cu (5 nm)/Py (8 nm)/Cu (10 nm)/Co (8 nm)/Ta (10 nm)/Cu (infinite) multilayer as a function of the angle φ between the magnetizations of the free Py and fixed Co layers, which is calculated from the Barnaś–Fert model (Ref. 15) $[\tau(\varphi)=-P(\varphi)\sin\varphi I\hbar/(2e)]$. Electrons flow from the Co layer to the Py layer for a positive current I.

transfer[15,23] (see Fig. 1). This so-called wavy angular dependence of the spin transfer torque (WAD-STT), which is characterized by a change of sign of the STT between 0 [parallel (P) configuration] and π [antiparallel (AP) configuration], arises from the modification of the spin accumulation profile in the structure caused by the different ratios of *thickness* to *spin diffusion length* of the magnetic layers. This WAD-STT modifies the stability of the static states P and AP: For one polarity of the current (positive current in our convention), both states are stabilized by the STT, whereas they are destabilized for the opposite polarity (negative current). In the latter case, it is predicted that the magnetization precesses even at zero external magnetic field. These predictions were validated experimentally by the present authors by measuring the microwave oscillations induced by the STT at zero (or low) applied field.[22]

In this article, we present a complete characterization and analysis of the magnetization dynamics in the presence of a WAD-STT. The results are compared to the prediction of the magnetization dynamics obtained by single domain magnetic simulations (macrospin approximation). We show that the main static and dynamical experimental features such as current-field phase diagram, variation of resistance with current, and variation of frequency with current and field can be reproduced by simulation at least qualitatively and, for some features, quantitatively. Therefore, the present work validates the diffusive models of the spin transfer that predict such WAD-STT.[14–17,24,25]

The paper is organized as follows. We first describe the predictions of the macrospin simulations by taking into account the WAD-STT. In Sec. II, we present the results of low field static and high frequency measurements obtained on a Co (8 nm)/Cu/Py (8 nm) nanopillar, in which a WAD-STT is predicted. These results are compared with the predictions of the macrospin simulations and discussed in Sec. III.

II. MACROSPIN SIMULATIONS WITH A WAVY ANGULAR DEPENDENCE OF THE SPIN TRANSFER TORQUE

A. Method

In this section, we present the results of the simulations of the magnetization dynamics of the Py free layer of a Co (8 nm)/Cu/Py (8 nm) trilayer by taking into account the *wavy* angular dependence of the torque. These calculations have been carried out in the macrospin approximation, i.e., by assuming the magnetization to be uniform during its motion. The magnetization of the Py free layer is described by a unit vector $\mathbf{m}=m_x\mathbf{u}_x+m_y\mathbf{u}_y+m_z\mathbf{u}_z$ and makes an angle φ with the magnetization of the Co layer which is supposed to be fixed and aligned along the x axis. As in experiments, the Py free layer has an elliptical cross section of 100×155 nm^2 and a thickness t_{Py} of 8 nm. It implies an in-plane uniaxial anisotropy field $\mathbf{H}_{\mathrm{an}}=H_{\mathrm{an}}m_x\mathbf{u}_x$ aligned along the direction of the long axis $\mathbf{u}_x$ of the ellipse and a demagnetizing field $\mathbf{H}_d=-H_d m_z\mathbf{u}_z$, with $\mathbf{u}_z$ perpendicular to the plane of the layers. The external field $\mathbf{H}_{\mathrm{app}}=H_{\mathrm{app}}\mathbf{u}_x$ is applied in the plane of the layer and aligned along the direction $\mathbf{u}_x$ of the uniaxial anisotropy field. The time dependent trajectory $\mathbf{m}(t)$ is found by solving the modified Landau–Lifschitz–Gilbert (LLG) equation including the STT $\boldsymbol{\tau}$, as follows:

$$\frac{d\mathbf{m}}{dt}=-\gamma_0\mathbf{m}\times\mathbf{H}_f+\alpha\mathbf{m}\times\frac{d\mathbf{m}}{dt}-\frac{\gamma_0}{\mu_0 M_s V}\boldsymbol{\tau}. \qquad (1)$$

Here, γ_0 is the absolute value of the gyromagnetic ratio, α is the Gilbert damping, M_s is the saturation magnetization, V is the volume of the Py nanomagnet, and $\mathbf{H}_f$ is an effective field which includes $\mathbf{H}_{\mathrm{app}}$, $\mathbf{H}_{\mathrm{an}}$, and $\mathbf{H}_d$. In order to characterize the influence of thermal activation on the magnetization dynamics, the simulations were carried out at both $T=0$ K and $T=300$ K. Thermal effects are simulated by introducing a randomly fluctuating field $\mathbf{H}_T$,[26,27] with $\mu_0\mathbf{H}_T=\sqrt{2k_BT\alpha/VM_s\gamma\Delta t}\mathbf{H}_{\mathrm{al}}$, where $\mathbf{H}_{\mathrm{al}}$ is a random Gaussian field with $\langle\mathbf{H}_{\mathrm{al}}\rangle=0$ and $\langle H_{\mathrm{al}}^2\rangle=1$, k_B is the Boltzmann constant, and Δt is the integration step. The magnetic parameters used for the simulations are described in the Appendix along with computational details. The spin transfer term is defined as $\boldsymbol{\tau}=P(\varphi)I\hbar/2e\,\mathbf{m}\times\mathbf{m}\times\mathbf{u}_{\mathbf{x}}$, where I is the current (defined as positive when the electrons flow from the fixed Co layer to the Py free layer) and e is the absolute value of the electron charge. The polarization factor $P(\varphi)$ is derived from the angular dependence of the torque calculated from the Barnaś–Fert model (see Fig. 1).

The displayed phase diagrams are constructed by calculating the mean values over the integration time of m_x and $\sigma_{mx}=\sqrt{\langle m_x^2-\langle m_x\rangle^2\rangle}$ after relaxation (σ_{mx} gives an evaluation of the amplitude of precession). These two quantities allow the determination of the borders between the different static and dynamical states. All presented simulations have been carried out for a positive current. No excitations are predicted by the simulations for a negative current.[28]

B. Results

1. $T=0$ K

The calculated variation of the frequency and the resistance with I for a zero applied field are shown in Figs. 2(a) and 2(b) (black curves) respectively. Starting from an initial P configuration and increasing current (plain line), the magnetization goes into sustained precession around the in-plane effective field (in-plane precession mode $\mathrm{IP_P}$) for a threshold

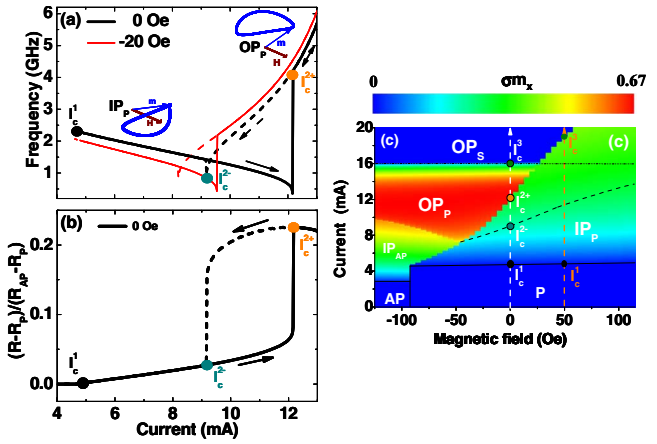

FIG. 2. (Color online) $T=0$ K. (a) Frequency of precession as a function of the current for several applied fields for increasing (plain line) and decreasing (dashed line) current. (b) Normalized resistance as a function of the current for $H=0$ for increasing (plain line) and decreasing (dashed line) currents. (c) Dynamical phase diagram for increasing current (σ_{mx} in color scale) and decreasing current (dashed and dotted line frontiers). For decreasing current, the dotted line corresponds to the frontier of the OP_S with the OP_P state and the dashed line corresponds to the frontier of the OP_P state with the IP_P state. The plain black lines define the frontiers of the P and AP states. The static and dynamical states are defined in the text.

current I_c^1 (black point at $I=4.8$ mA) with a precession frequency ($f=2.28$ GHz) close to Kittel's frequency of the ferromagnetic (FMR) small angle precession ($f=2.23$ GHz). When the current is increased above I_c^1, the angle of precession increases but the frequency decreases ("redshift regime"). This behavior, i.e., the decrease of frequency with increasing current, is a nonlinear effect due to the dependence of the frequency on the precession amplitude.[29–31] In this mode, only a small increase of the resistance with increasing current is predicted, although a large angle precession can be reached. For a threshold current I_c^{2+} (orange point at $I=12$ mA), the magnetization dynamics abruptly changes to an out-of-plane precession mode (labeled as OP_P). This transition is associated with a jump in frequency and a large increase in the resistance. In this OP_P regime, the magnetization precesses around the demagnetizing field and the frequency is set by the mean out-of-plane component of magnetization $\langle m_z \rangle$. For increasing current, the trajectory goes away from the plane of the layer (higher $\langle m_z \rangle$) and the frequency increases ("blueshift regime"). For higher current ($I>13$ mA, not shown), the magnetization precesses faster (up to 20 GHz) around circular trajectories of decreasing radius while current is increased. These trajectories converge for even higher current to a quasistatic out-of-plane state OP_S. As shown in Figs. 2(a) and 2(b), the transition between the IP_P and the OP_P precession modes is irreversible: The critical current for this transition is higher for increasing current (I_c^{2+}, orange point and plain line) than for decreasing current (I_c^{2-}, blue point and dashed line), which results in hysteretic $R(I)$ and $f(I)$ curves.

In addition, the variation of the frequency with I for a lower field $H=-20$ Oe is plotted in Fig. 2(a) (red curve). In the IP_P mode, the black curve ($H=0$ Oe) is above the red curve ($H=-20$ Oe): The frequency increases with the field. On the contrary, in the OP_P mode, the black curve is below the red curve and the frequency decreases with the field: The in-plane field pulls the magnetization in the plane of the layer, decreasing $\langle m_z \rangle$ and therefore the frequency.

In Fig. 2(c), we present a calculated current-field dynamical phase diagram for increasing current starting from an initial P configuration. The amplitude of precession (σ_{mx}) is plotted on a color scale. Several regimes can be defined. First, at high positive field ($H>+25$ Oe) [see the orange dashed line in Fig. 2(c)], only the IP_P mode is observed for $I_c^1<I<I_c^3$. For $I>I_c^3$, the magnetization goes into the quasistatic out-of-plane precession state OP_S. In a second regime at low field, i.e., smaller than the coercive field [see the white dotted line in Fig. 2(c)], the out-of-plane precession mode OP_P appears for I above I_c^{2+} with $I_c^1<I_c^{2+}<I_c^3$. The amplitude of precession (red color) and therefore the emitted power are maximum in this mode. In addition, the aforementioned hysteretis leads to different frontiers for increasing current (colored frontier) and decreasing current (dotted line for the OP_S to OP_P transition and dashed lines for the IP_P to OP_P transition. At higher current and field ($H>+25$ Oe), the transition to the OP_S state is also irreversible: Magnetization switches from IP_P to OP_S for increasing current (colored frontiers) and from OP_S to OP_P (dotted lines) for decreasing current.

Finally, for a lower applied field ($H<-50$ Oe), before reaching the OP_P mode, the magnetization first precesses in plane around the AP state (mode denoted as IP_{AP}). Note that in this mode, the frequency decreases with current and increases with (positive) field. Starting from an initial AP state ($H<-90$ Oe), this precession state IP_{AP} is first observed when the current is increased from zero.

To summarize, the magnetization dynamics for a WAD-STT is very different from the one predicted for a standard angular dependence of the STT.

(a) For $H>H_c$, where H_c is the coercive field of the free layer, the precession modes are predicted for a positive current for a WAD-STT structure in our current convention, whereas they are obtained for a negative current for a standard structure.

(b) For $H<H_c$, in the *standard* case, only small angle IP_P precessions around the in-plane effective field are predicted in a very narrow range of current before the magnetization switches to the other stable static state (P or AP) due to the increase of the precession amplitude with current.[32,33] In the case of a WAD-STT, both static states (P or AP) are destabilized by the STT and this in-plane precession mode is present on a much larger range of current. In a similar manner to what is observed for a *standard* angular dependence at high field, large angle in-plane trajectories bifurcate into out-of-plane trajectories at higher current.[31,33] One can note that this large angle out-of-plane precession is predicted even in the absence of an external field in a WAD-STT structure. It is therefore possible to emit microwaves at zero field, only by injecting a current in the structure.

2. $T=300$ K

The main effect of temperature is the almost complete disappearance of the irreversibility associated with the tran-

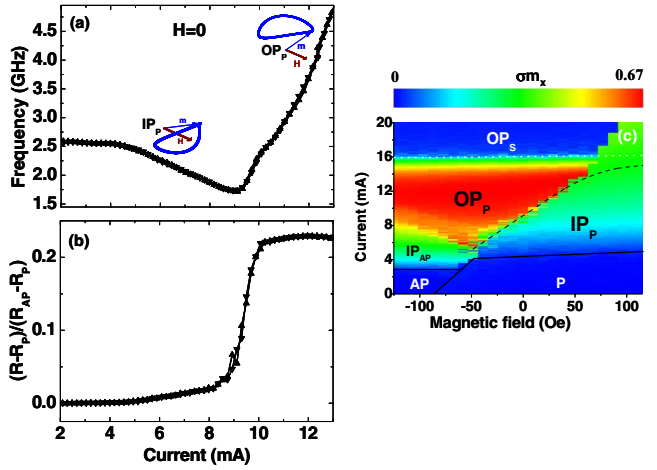

FIG. 3. (Color online) $T=300$ K. (a) Frequency of precession and (b) normalized resistance as a function of the current for increasing (up triangles) and decreasing (down triangles) current for $H=0$. (c) Dynamical current-field phase diagram for increasing current (σ_{mx} in color scale) and the decreasing current (dashed and dotted line frontiers).

sition from the IP_P to the OP_P precession mode. The thermal energy allows the magnetization to go across the energy barrier that separates these two states. This appears in the phase diagram of Fig. 3(c): The frontiers between the two states are quasi-identical for increasing (colored frontier) or decreasing current (dashed lines) except at a large applied field ($H>60$ Oe). As a consequence, this reversible behavior leads to an expansion of the current-field region, in which the OP_P precession mode occurs: For a given value of the applied field, the critical current for the transition from IP_P to OP_P is lower at $T=300$ K compared to the 0 K values.[34] The reversibility of this transition results in nonhysteretic $f(I)$ and $R(I)$ curves, as shown in Figs. 3(a) and 3(b).[35] The effect of thermal energy appears, in particular, in the transition zone between the two states and especially for currents close to the minimum in frequency ($I\approx 9.1$ mA). In this zone, the thermal energy makes the system unstable and a telegraph noise with a characteristic time of about 10 ns is observed between the state IP_P and the two degenerated out-of-plane trajectories which are symmetrical around the (xy) plane. To conclude this section, the temperature does not modify the main characteristics of the dynamics in a WAD-STT structure, such as a steady precession at zero external field.

III. EXPERIMENTAL RESULTS AND COMPARISON WITH MACROSPIN SIMULATIONS

We present a detailed experimental characterization of the magnetization dynamics induced by STT in a Co (8 nm)/Cu (10 nm)/Py (8 nm) nanopillar, in which a WAD-STT is predicted. This dynamics was studied by measuring the high frequency voltage oscillations generated by the magnetization precession with a spectrum analyzer after amplification. To directly compare the experimental results with the simulations, we consider for experiments an effective external field H_{eff} that takes into account the contribution from the dipolar field exerted on the Py free layer ($H_{\text{dip}}\approx -43$ Oe).

A. Initial configuration: P

In Fig. 4(a), we display the microwave spectra measured for several values of injected current and a fixed effective applied field $H_{\text{eff}}=-62$ Oe. The corresponding variation of the frequency with I at this field is plotted in Fig. 4(b). The analysis of the frequency dependence with the current allows the definition of three different dynamical regimes. In the low current range ($4\ \text{mA}\leq I\leq 9$ mA), we observe that the frequency increases with I, i.e., a blueshift with I (regime 1). Then, it stays approximately constant for $9\ \text{mA}\leq I\leq 10$ mA) (regime 2). At higher current ($I>10$ mA), a slight decrease in frequency with I is observed, i.e., a redshift with I (regime 3).[36] Three corresponding behaviors are observed in the frequency dependence with H_{eff}, as illustrated in Fig. 4(c), by the microwave spectra measured for a constant current of 10 mA and several values of the applied field. The corresponding frequencies are plotted in Fig. 4(d). In the low field range ($-47\leq H_{\text{eff}}\leq 2$ Oe), the frequency decreases with H_{eff} (regime 1). For higher negative fields ($-62\leq H_{\text{eff}}\leq -47$ Oe), the frequency remains approximately constant ($f\approx 3.5$ GHz) with H_{eff} (regime 2). Then, in a narrow experimental window for H_{eff} close to the switching field, the frequency decreases with the field ($H_{\text{eff}}<-62$ Oe) (regime 3).

In Fig. 4(e), we present a current-field dynamical phase diagram with the microwave power plotted in color scale. As predicted by the model, the microwave power is emitted for a *positive* current and at low H_{eff} ($H_{\text{eff}}<30$ Oe), i.e., smaller than the coercive field, and, in particular, at *zero* H_{eff}. This behavior is very different from the one typically observed in standard structures, where steady precession associated with microwave emission is observed at *high* H_{eff}, and for a *negative* current.[5,37] In addition, in Fig. 4(e), we plot the frontiers between the different dynamical regimes presented above in plain lines.[38] In regime 1, the frequency increases with I and decreases with H_{eff}. It is present in the largest part of the region of the phase diagram where the microwave power is measured. This behavior is indeed the only one observed at low current (from $I\geq 4$ mA) and close to the zero effective field. The regime 2 appears at low H_{eff} and for higher currents. It is characterized by a frequency that remains approximately constant with I and also with the applied field. Finally, the regime 3 in which the frequency slightly decreases with I (and increases with H_{eff}) is observed in the top-left corner of the diagram corresponding to large currents and applied fields close to the switching field ($H_{\text{eff}}\approx -90$ Oe).

We can directly compare the experimental results to the simulated dynamical phase diagram shown in Fig. 4(f). The current-field region in which an out-of-plane precession OP_P mode is predicted [red color in Fig. 4(f)] coincides with the zone in which the high frequency power is measured (dynamical regimes 1, 2, and 3). Note that the field dependence of the experimental critical currents is in excellent agreement with the one associated with the IP_P/OP_P transition in the simulations. In addition, no microwave power was measured in the region where an IP_P mode is predicted. We believe

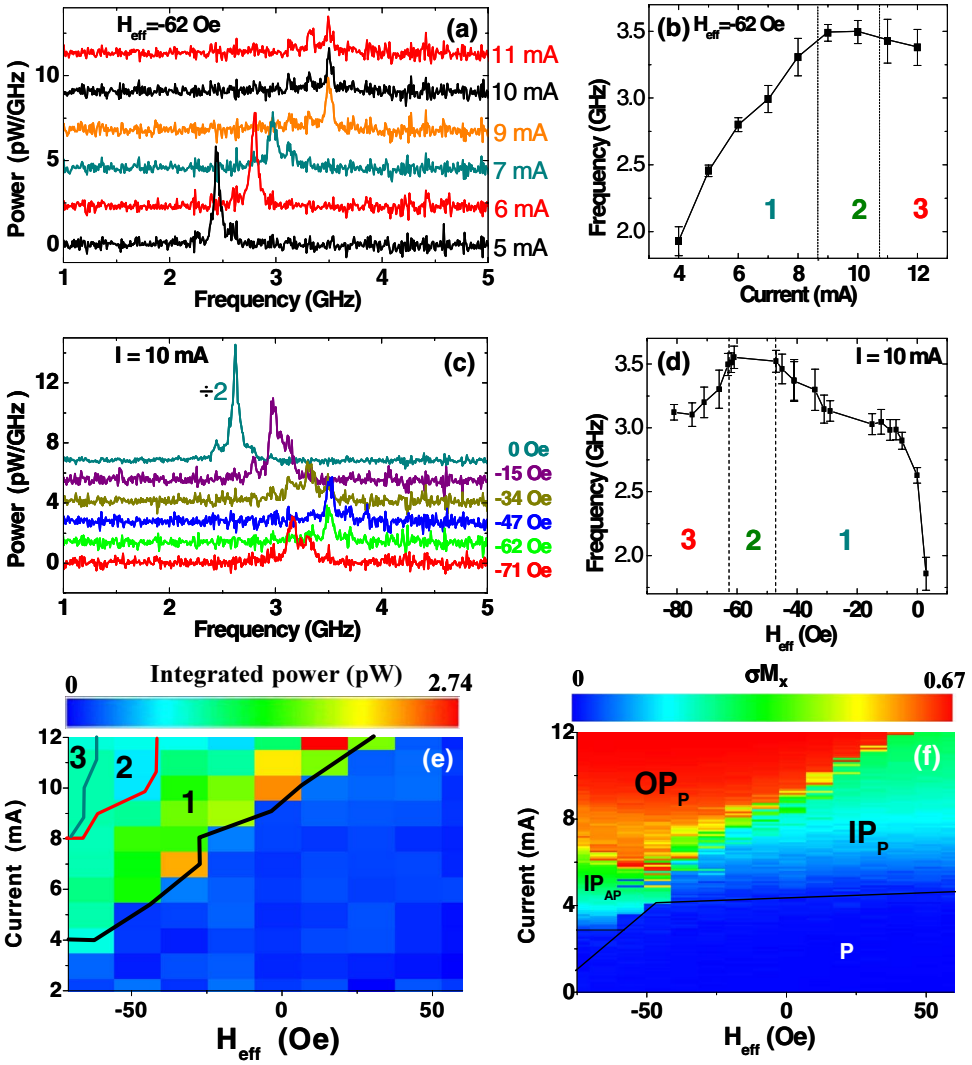

FIG. 4. (Color online) (a) Microwave power spectra for several values of injected current and $H_{\text{eff}}=-63$ Oe. (b) Frequency associated with the peaks in the microwave spectra as a function of current for $H_{\text{eff}}=-63$ Oe. (c) Microwave power spectra for several values of H_{eff} and $I=10$ mA. (d) Frequency associated with the peaks in the microwave spectra as a function of H_{eff} for $I=10$ mA. H_{eff} is defined as $H_{\text{eff}}=H_{\text{app}}+H_{\text{dip}}$, with $H_{\text{dip}}=-43$ Oe. In (b) and (d), the error bars correspond to the linewidth of the peak. (e) Experimental dynamical current-field phase diagram for increasing current starting from an initial P state. The microwave power is plotted in color scale. The dynamical regimes denoted as 1, 2, and 3 are defined in the text. (f) Simulated current-field phase diagram for increasing I starting from an initial P state. The amplitude of oscillation (σ_{mx}) is plotted in color scale.

that, most probably, the weak microwave emission associated with this IP_P mode in a WAD-STT structure is too small to be measured with our experimental setup (this point will be discussed in Sec. IV). Finally, the predicted IP_{AP} precession mode in the lower left corner of the diagram characterized by a redshift regime with the current and moderate precession amplitude was not experimentally observed.

B. Initial configuration: AP

We can go deeper into the compared analysis of experiments and simulations by looking at some additional features observed when one starts from the AP configuration. In Figs. 5(a) and 5(b), we show the experimental and the simulated phase diagrams, respectively, for an increasing current starting from an initial AP configuration. The experimental diagram was deduced from several $R(I)$ curves for different values of the applied field. The resistance level is plotted in color scale in Fig. 5(a) and the corresponding $R(I)$ curves are plotted in Fig. 5(c). Experimentally, starting from the AP configuration and above a positive threshold current, the magnetization switches sharply from the AP to the P configuration. Then, for a larger current, an increase of the resistance is observed due to the onset of a steady precession mode. This behavior is well reproduced by the macrospin simulation [see Fig. 5(b)]. In particular, the critical currents associated with the magnetization switching from the AP to the P state are well reproduced, as well as their dependence on the applied magnetic field.

A good agreement is obtained between the corresponding experimental [Fig. 5(c)] and simulated [Fig. 5(d)] $R(I)$ curves obtained for increasing current starting from an initial AP configuration (see, for example, the critical currents or the variation of resistance). In particular, the simulated increase of resistance associated with the transition from the IP_P to the OP_P state is reversible, as is the case in experiments. If one calculates the differential resistance $dV/dI=R+IdR/dI$ using the simulated $R(I)$ curves, one observes that this transition is associated with a peak in the $dV/dI(I)$ curves. This reproduces the experimental observations where such peaks, which characterize the reversibility of the transition, have always been observed at the onset of the microwave emission (see Ref. 22). In addition, for both simulations and experiments, no significant variation for the resistance is observed for the in-plane precession IP_P mode. However, the simulation overestimates the stability of the IP_{AP} precession mode around the AP configuration at the

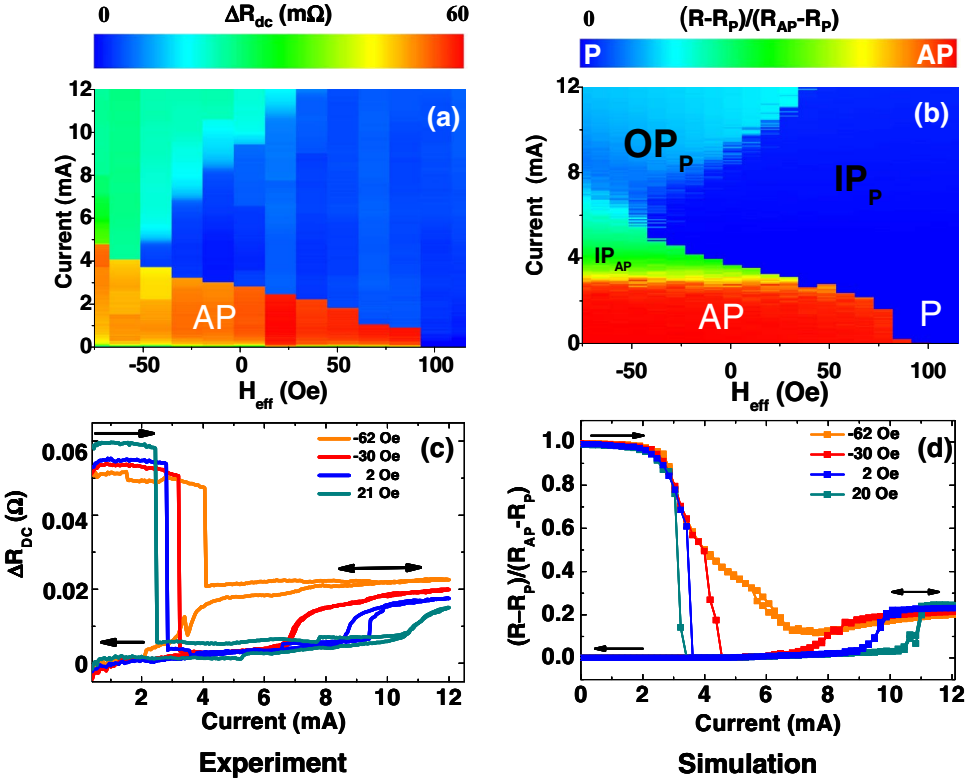

FIG. 5. (Color online) (a) Experimental current-field phase diagram for increasing current starting from an initial AP state. The normalized resistance of the sample ΔR is plotted in color scale. (b) Corresponding simulated phase diagram (normalized resistance in color scale). (c) Measured resistance as a function of the current for several values of H_{eff} starting from an initial AP state for successively increasing and decreasing current. (d) Corresponding simulated normalized resistance vs current curves. The experimental normalized resistance ΔR is obtained by subtracting from the experimental R versus I curves a reference curve to remove the changes in resistance due to Joule heating.

expense of the P state [see the IP_{AP} zone in Figs. 5(b) and 5(d)]. This can be explained by an underestimation of the effect of temperature caused by a sweeping ramp 10^5 faster in simulations than in experiments. With a slower current ramp, the IP_{AP} mode should be more unstable and thus the reversal toward the P state should be favored. This may also explain why we did not measure the microwave power associated with this dynamical precession mode.

C. Frequency of the precession

In Fig. 6(a), we compare the experimental and calculated $f(I)$ curves for several values of the applied field. A good agreement is obtained for fields close to zero effective field (H_{eff}=2 and 10 Oe) corresponding to the regime 1 in the phase diagram. In particular, the blueshift with I and the decrease of frequency with H_{eff}, which is experimentally observed, is well reproduced by the simulation. The simulations and experiments significantly differ for a higher negative field (H_{eff}=−45 Oe). In particular, the saturation regime (regime 2) characterized by a frequency approximately constant with I is not reproduced by the simulation. However, the experimental slope of the frequency with the current df/dI before saturation [H_{eff}=−45 Oe ($7 \leq I \leq 9$ mA), H_{eff} =2 Oe, and H_{eff}=10 Oe] is well reproduced by the simulations. This seems to indicate that the regime before saturation (regime 1) is closer to a homogeneous precession mode than the regimes observed for higher currents (regimes 2 and 3).

The disagreement between simulations and experiments of the $f(I)$ curve at a high negative field reflects a decrease in frequency with H_{eff} that is lower in simulations than in experiments. This appears in Figs. 6(b) and 6(c), where the experimental and simulated dependences of the frequency on the magnetic field are compared for I=10 and 11 mA. However, the general shape of the experimental $f(H)$ curve in the redshift regime for higher field values is qualitatively reproduced by the simulation.

IV. DISCUSSION

The macrospin simulations reproduce the following main experimental features well: the region in the current-field

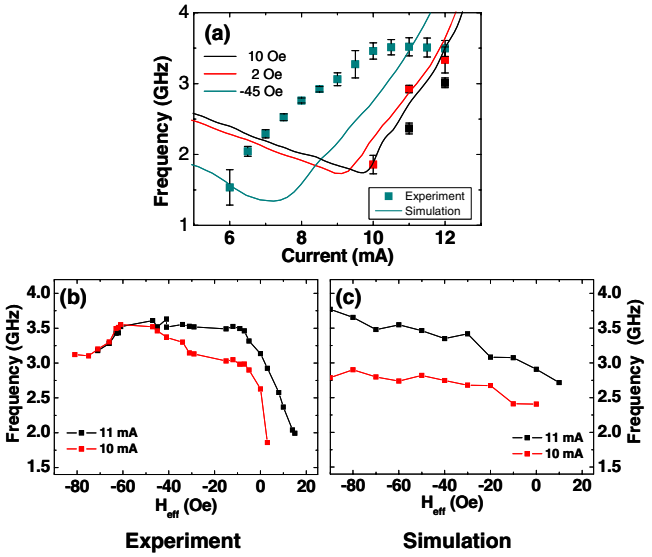

FIG. 6. (Color online) (a) Simulated (plain lines) and experimental (square points) variations of frequency with the current for several values of H_{eff}. (b) Simulated and (c) experimental variations of frequency with H_{eff} for I=10 mA and I=11 mA.

diagram with larger power emission and increased resistance, the frontiers between the main different static and dynamical states, and the dc resistance of these different states. This agreement is quite satisfactory if we consider the crude macrospin approximation that was used.

The direct comparison of the experimental and simulated dynamical phase diagrams clearly suggests that the observed excitations are associated with an out-of-plane precession mode. This is confirmed by the blueshift in I and the redshift in H_{eff} observed in the dynamical regime 1, which is a signature of this dynamical mode. However, the macrospin simulations do not reproduce the saturation regimes observed at low H_{app} and for a large current (regimes 2 and 3) [see Fig. 6(a)]. We believe that these regimes are probably associated with dynamical modes characterized by an inhomogeneous distribution of magnetization. It is worth noting that the only other two groups who observed a blueshift regime for an in-plane applied field also observed this saturation of (or decrease in) the frequency for a larger I (see Fig. 3 of Refs. 37 and 39), suggesting the intrinsic character of this dynamical feature. On the basis of micromagnetic simulations,[39] it has recently been suggested that this behavior can be attributed to the onset of inhomogeneous dynamical modes characterized by a mean out-of-plane component of magnetization $\langle m_z \rangle$, which is lower than that for the uniform mode. The onset of such modes leads to a decrease in the large magnetostatic energy generated by the strong demagnetizing field when the magnetization goes out of the film plane. Since the frequency of precession is proportional to $\langle m_z \rangle$, the decrease in $\langle m_z \rangle$ results in a decrease in the frequency as compared to the macrospin prediction and thus explains this saturation phenomenon. The in-plane Oersted field may also play a role: In the case of an out-of-plane precession mode, it tends to pull the magnetization toward the film plane. This also leads to a decrease in the precession frequency.[40]

Another point to discuss is the nonobservation of a redshift regime associated with the $\mathrm{IP_P}$ mode in our experiments. This regime was indeed observed in a nanopillar having a different WAD-STT structure, i.e. Co (4 nm)/Cu/Py (8 nm). In this nanopillar, before the onset of the higher power blueshifting microwave peaks, signals of very low amplitude presenting a clear redshift behavior have been observed. In standard nanopillars, such redshifting signals that can be associated with a large angle $\mathrm{IP_P}$ mode generally go with a large emitted power.[5,41] This difference between standard and WAD-STT samples can be explained by a weaker slope of the angular dependence of the GMR for angles around $\varphi=0$ in the case of a WAD-STT.[42] This results in a weak variation of the resistance (and therefore a very weak power) for in-plane oscillations of magnetization even for large angles. In our calculations, we accounted for this specific angular dependence of the GMR by using a normalized resistance $r(\varphi)=\sin^2(\varphi/2)/[1+\chi\cos^2(\varphi/2)]$ with an asymmetry factor[42] $\chi=7.7$. As can be seen in Fig. 3(b) or 5(d), this results in a low increase in the resistance of the device in the $\mathrm{IP_P}$ mode. To evaluate the influence of the angular dependence of the GMR on the emitted power, we calculated the maximum emitted power for this $\mathrm{IP_P}$ mode using Eq. (A1) with $\chi=7.7$, $\chi=2$ [experimentally measured by Urazhdin *et al.*[20] in a standard structure Py (6 nm)/Cu/Py (12 nm), and $\chi=0$], which corresponds to the simple angular dependence $\Delta R=(1-\cos\theta)/2$. The simulated power in the precession mode for $\chi=7.7$ is about 10 times lower than that for $\chi=2$ and 25 times lower than that for $\chi=0$. If this assumption is valid, then it allows us to explain that in our experimental configuration, the measured signals in this $\mathrm{IP_P}$ precession mode were too weak to be detected.

Finally, our simulations allow the calculation of the output power in the $\mathrm{OP_P}$ mode: It is about 3.9 $\mathrm{pW/mA^2}$, which is to be compared with the maximum measured output power of about 4.5×10^{-2} $\mathrm{pW/mA^2}$, i.e., approximately a factor of 80 smaller. This discrepancy may arise from several factors. First, due to the impedance mismatch, the attenuation of the signal in the high frequency line and the variation of the amplification gain with frequency, the measured signal (after taking the amplification into account) is only a fraction of the actual emitted signal. Second, the fact that the $\mathrm{OP_P}$ mode predicted by the macrospin simulation has been rarely observed experimentally[5] indicates that the macrospin approximation does not properly describe the dynamics in this precession mode. Recently, micromagnetic calculations[43,44] have shown that this dynamical $\mathrm{OP_P}$ mode is sensitive to the magnetization homogeneity. Factors that favor the inhomogeneity, such as temperature or the Oersted field, decrease the output power in this precession mode. Third, the possible presence of ferromagnetic oxides (NiO) on the sidewalls of the pillar due to air exposure during the fabrication process[45] or the stronger Oersted field on the edges may force the magnetization to lie in the plane on the edges. In this case, only a part of the magnetization in the center of the magnet precesses in the out-of-plane direction resulting in a weaker output power.

V. CONCLUSION

We have simulated in the macrospin approximation the magnetization dynamics induced by a STT with a "wavy" angular dependence predicted for a Co (8 nm)/Cu/Py (8 nm) nanopillar by the Barnaś–Fert model.[15,22,23] At low H_{eff}, the magnetization dynamics is strongly modified as compared to a standard angular dependence of the torque. When the current is increased at low and even zero applied fields, one successively observes an in-plane precession mode ($\mathrm{IP_P}$), in which the frequency decreases with I (redshift regime) and an out-of-plane precession mode ($\mathrm{OP_P}$), in which the frequency increases with the current (blueshift regime). The transition between both regimes is associated with an increase in the dc resistance and a strong increase in the output power. We have presented some experimental results that confirm this zero and low field steady precession. In the main part of the current-field phase diagram at low H_{eff}, the frequency increases with I (blueshift regime) and decreases with H_{eff}. In the remaining part of the diagram (applied field close to the switching field and high applied current), a regime in which the frequency is approximately constant (or decreases slightly) with I is observed. The macrospin simulations reproduce the observed main experimental features [phase diagram, $R(I)$ curves, and dependence of frequency with the current and the field] and suggest that the dynamical

excitations, which are experimentally observed are associated with an out-of-plane precession mode. However, the saturation regimes observed at lower H_{eff} and higher I are not reproduced by the simulation and may reveal the onset of inhomogeneous dynamical excitations. The general good agreement between models and experiments confirms the predicted WAD-STT in this structure[15,22] and validate the diffusive models of the spin transfer that predict such WAD-STT.[14–17,24,25] By playing on the distribution of spin relaxation in the structure, it is therefore possible to strongly modify the STT and the magnetization dynamics induced by the torque. This possibility of engineering the angular dependence of the torque with different spin diffusion lengths in the magnetic layers underlines the role of the spin accumulation and the spin relaxation effects on the STT.

ACKNOWLEDGMENTS

We would like to thank L. Vila for assistance with fabrication, H. Hurdequint for FMR measurements, and O. Copie and B. Marcilhac for assistance with transport and frequency measurements. This work was partly supported by the Centre National de la Recherche Scientifique (CNRS), by the French National Agency of Research ANR through the PNANO program (MAGICO 05-044-02) and (NanoMASER 06-067-04), and by the EU through the Marie Curie Training network SPINSWITCH (MRTN-CT-2006-035327). We have used the multilayer code developed by H. Jaffrès (henri.jaffres@thalesgroup.com) for the CPP-GMR and spin transfer torque calculations.

APPENDIX: PARAMETERS USED FOR THE MACROSPIN SIMULATION

For the macrospin simulation a gyromagnetic ratio $\gamma_0 = 2.2 \times 10^5$ m$(\text{A}^{-1}\,\text{s}^{-1})$ has been used. The saturation magnetization $\mu_0 M_S = 0.87$ T, has been deduced from ferromagnetic resonance experiments carried out on Cu (6 nm)/Py (7 nm)/Cu (6 nm) thin films. The anisotropy fields H_d and H_{an} can be expressed as a function of demagnetizing factors N_x, N_y, and N_z, which are associated with the shape of the nanomagnet with $H_d \approx M_s(N_z - N_y)$ and $H_{\text{an}} \approx M_s(N_y - N_x)$. If we approximate the shape of the nanomagnet with an ellipsoid with axes of 150, 105, and 8 nm close to the lateral dimensions measured by scanning electron microscopy (SEM) within the measurement uncertainty, one obtains[46] $N_x = 0.047$, $N_y = 0.063$, and $N_z = 0.89$, which lead to $\mu_0 H_d \approx 0.7$ T and $\mu_0 H_{\text{an}} \approx 0.014$ T. This value of H_{an} is close to the anisotropy field $\mu_0 H'_{\text{an}} \approx 0.0145$ T, which one can estimate from the room temperature experimental coercive field H_c.[47] For a direct comparison between experimental and theoretical phase diagrams, the uniaxial anisotropy field H_{an} was adjusted to obtain a simulated coercive field equal to the experimental one ($\mu_0 H_c = 0.009$ T). For simulation at $T = 0$ K, we therefore used $\mu_0 H_{\text{an}} = 0.009$ T. At $T = 300$ K and with the parameters and waiting time used in the simulation, one obtains $\mu_0 H_{\text{an}} = 0.012$ T. A Gilbert damping parameter $\alpha = 0.018$ has been used. Finally, currents are deduced from current densities using a lateral surface of the nanopillar of $A = 1.38 \times 10^{-14}$ m^2, which are experimentally measured by SEM. Since the angular dependence of the GMR in a WAD-STT structure is predicted[17,42] to significantly deviate from the commonly used dependence $\sin^2(\varphi/2)$, the normalized magnetoresistance $r = (R - R_{\text{P}})/(R_{\text{AP}} - R_{\text{P}})$ was calculated using the following relation:[18,19]

$$r(\varphi) = \sin^2(\varphi/2)/[1 + \chi \cos^2(\varphi/2)]. \tag{A1}$$

We have used $\chi = 7.7$ that was experimentally derived by Urazhdin *et al.*[42] in a nonsymmetrical pillar composed of Py (6 nm)/Cu (10 nm)/Py (1.5 nm) for which a WAD-STT is also predicted.

The precession frequency was derived from the higher amplitude lowest order peak in the Fourier transform spectrum of the m_y component. In the case of a slight misalignment between the magnetization of the polarizing layer and the easy axis of the free layer, this frequency actually corresponds to the one of the lowest order peak in the microwave spectra experimentally measured.[48,49] The output power P corresponding to the simulated trajectories is deduced from the reduced resistance r using $P/I^2 = \Delta R^2_{\text{expt}}/Z_c \cdot \langle (r - \langle r \rangle)^2 \rangle$, with $\Delta R_{\text{expt}} = R_{\text{AP}} - R_{\text{P}} = 51$ mΩ as the experimental static variation of resistance due to the GMR and $Z_c = 50$ Ω as the characteristic impedance of the high frequency line. $\langle \cdots \rangle$ indicates the mean value of 40 ns after relaxation of the magnetization.

The LLG equation [Eq. (1)] has been solved using a fourth order Runge–Kutta algorithm with a time step of 1 ps. For simulation at $T = 0$ K, to let the magnetization reach a stationary state, a 100 ns relaxation time has been used. Then, trajectories are saved over 40 ns. These trajectories are used for the fast Fourier transform calculations and the deduction of the magnetoresistance. For simulation at $T = 300$ K after application of the current, a relaxation time of 30 ns has been used and simulations have been carried out with a current sweep ramp of 10^5 mA/s. The plotted frequency and resistance vs current curves are averaged over five realizations or more.

*Present address: Universität Konstanz, Universitätstrasse 10, D-78457 Konstanz, Germany; olivier.boulle@uni-konstanz.de

†Corresponding author; vincent.cros@thalesgroup.com

‡Present address: Instituto de Fisica, UFRGS, 91501-970 Porto Alegre, RS, Brazil.

[1] J. C. Slonczewski, J. Magn. Magn. Mater. **159**, L1 (1996).

[2] L. Berger, Phys. Rev. B **54**, 9353 (1996).

[3] J. A. Katine, F. J. Albert, R. A. Buhrman, E. B. Myers, and D. C. Ralph, Phys. Rev. Lett. **84**, 3149 (2000).

[4] J. Grollier, V. Cros, A. Hamzic, J. M. George, H. Jaffrès, A. Fert, G. Faini, J. B. Youssef, and H. Legall, Appl. Phys. Lett. **78**, 3663 (2001).

[5] S. I. Kiselev, J. C. Sankey, I. N. Krivorotov, N. C. Emley, R. J. Schoelkopf, R. A. Buhrman, and D. C. Ralph, Nature(London) **425**, 380 (2003).
[6] W. H. Rippard, M. R. Pufall, S. Kaka, S. E. Russek, and T. J. Silva, Phys. Rev. Lett. **92**, 027201 (2004).
[7] M. D. Stiles and A. Zangwill, Phys. Rev. B **66**, 014407 (2002).
[8] A. Brataas, G. E. W. Bauer, and P. J. Kelly, Phys. Rep. **427**, 157 (2006).
[9] X. Waintal, E. B. Myers, P. W. Brouwer, and D. C. Ralph, Phys. Rev. B **62**, 12317 (2000).
[10] T. Valet and A. Fert, Phys. Rev. B **48**, 7099 (1993).
[11] Q. Yang, P. Holody, S.-F. Lee, L. L. Henry, R. Loloee, P. A. Schroeder, W. P. Pratt, Jr., and J. Bass, Phys. Rev. Lett. **72**, 3274 (1994).
[12] M. D. Stiles and A. Zangwill, J. Appl. Phys. **91**, 6812 (2002).
[13] J. Xiao, A. Zangwill, and M. D. Stiles, Eur. Phys. J. B **59**, 415 (2007).
[14] A. Fert, V. Cros, J.-M. George, J. Grollier, H. Jaffrès, A. Hamzic, A. Vaurès, G. Faini, J. B. Youssef, and H. Le Gall, J. Magn. Magn. Mater. **272–276**, 1706 (2004).
[15] J. Barnaś, A. Fert, M. Gmitra, I. Weymann, and V. K. Dugaev, Phys. Rev. B **72**, 024426 (2005).
[16] A. A. Kovalev, A. Brataas, and G. E. W. Bauer, Phys. Rev. B **66**, 224424 (2002).
[17] J. Manschot, A. Brataas, and G. E. W. Bauer, Phys. Rev. B **69**, 092407 (2004).
[18] J. C. Slonczewski, J. Magn. Magn. Mater. **247**, 324 (2002).
[19] A. Manchon and J. C. Slonczewski, Phys. Rev. B **73**, 184419 (2006).
[20] S. Urazhdin, N. O. Birge, W. P. Pratt, Jr., and J. Bass, Appl. Phys. Lett. **84**, 1516 (2004).
[21] M. AlHajDarwish, H. Kurt, S. Urazhdin, A. Fert, R. Loloee, W. P. Pratt, Jr., and J. Bass, Phys. Rev. Lett. **93**, 157203 (2004).
[22] O. Boulle, V. Cros, J. Grollier, L. G. Pereira, C. Deranlot, F. Petroff, G. Faini, J. Barnas, and A. Fert, Nat. Phys. **3**, 492 (2007).
[23] J. Barnas, A. Fert, M. Gmitra, I. Weymann, and V. Dugaev, Mater. Sci. Eng., B **126**, 271 (2006).
[24] J. Manschot, A. Brataas, and G. E. W. Bauer, Appl. Phys. Lett. **85**, 3250 (2004).
[25] M. Gmitra and J. Barnaś, Phys. Rev. Lett. **96**, 207205 (2006).
[26] W. F. Brown, Jr., Phys. Rev. **130**, 1677 (1963).
[27] S. E. Russek, S. Kaka, W. H. Rippard, M. R. Pufall, and T. J. Silva, Phys. Rev. B **71**, 104425 (2005).
[28] According to our notation, the electrons go from the Co fixed layer to the NiFe free layer for a positive current. Note that the excitations of the parallel state by a positive current are contrary with the standard situation in which a negative current excites the parallel state.
[29] A. N. Slavin and P. Kabos, IEEE Trans. Magn. **41**, 1264 (2005).
[30] S. M. Rezende, F. M. de Aguiar, and A. Azevedo, Phys. Rev. Lett. **94**, 037202 (2005).
[31] G. Bertotti, C. Serpico, I. D. Mayergoyz, A. Magni, M. d'Aquino, and R. Bonin, Phys. Rev. Lett. **94**, 127206 (2005).
[32] J. Z. Sun, Phys. Rev. B **62**, 570 (2000).
[33] M. Stiles and J. Miltat, in *Spin Dynamics in Confined Magnetic Structures III*, edited by B. Hillebrands and A. Thiaville (Springer-Verlag, Berlin, Heidelberg, 2006).
[34] We found that this decrease is not due to the different values of H_{an} used for $T=0$ K and $T=300$ K.
[35] At low I below I_c^1, the plotted frequency corresponds to a small elliptical precession of magnetization induced by thermal fluctuations whose frequency (2.58 GHz) is equal to the Kittel FMR frequency (2.58 GHz). The small variation of the frequency observed at low I for the in-plane precession mode between 0 and 300 K is due to the higher anisotropy field used in the simulation for $T=300$ K ($H_{an}=120$ Oe instead of 90 Oe).
[36] This decrease appears more clearly at an even lower field ($H_{eff} \leq -75$ Oe) close to the switching field (not shown).
[37] S. I. Kiselev, J. C. Sankey, I. N. Krivorotov, N. C. Emley, A. G. F. Garcia, R. A. Buhrman, and D. C. Ralph, Phys. Rev. B **72**, 064430 (2005).
[38] These frontiers were constructed by considering the dependence of the emission frequency with I at a fixed field from more than a hundred microwave spectra. Similar frontiers are obtained if the phase diagram is constructed from the dependence of the emission frequency with H_{eff} at a fixed current (not shown).
[39] D. Houssameddine, U. Ebels, B. Delaët, B. Rodmacq, I. Firastrau, F. Ponthenier, M. Brunet, C. Thirion, J.-P. Michel, L. Prejbeanu-Buda, M.-C. Cyrille, O. Redon, and B. Dieny, Nat. Mater. **6**, 447 (2007).
[40] G. D. Loubens, Ph.D. thesis, Universite Paris XI, 2005.
[41] J. C. Sankey, I. N. Krivorotov, S. I. Kiselev, P. M. Braganca, N. C. Emley, R. A. Buhrman, and D. C. Ralph, Phys. Rev. B **72**, 224427 (2005).
[42] S. Urazhdin, R. Loloee, and W. P. Pratt, Jr., Phys. Rev. B **71**, 100401(R) (2005).
[43] D. V. Berkov and N. L. Gorn, Phys. Rev. B **72**, 094401 (2005).
[44] I. N. Krivorotov, D. V. Berkov, N. L. Gorn, N. C. Emley, J. C. Sankey, D. C. Ralph, and R. A. Buhrman, Phys. Rev. B **76**, 024418 (2007).
[45] N. C. Emley, I. N. Krivorotov, O. Ozatay, A. G. F. Garcia, J. C. Sankey, D. C. Ralph, and R. A. Buhrman, Phys. Rev. Lett. **96**, 247204 (2006).
[46] J. A. Osborn, Phys. Rev. **67**, 351 (1945).
[47] The coercive field H_c at a temperature T can be expressed as a function of the uniaxial anisotropy field H'_{an} (Ref. 50) $H_c(H'_{an}) = H_{an}(1-[k_BT/E_k \ln(f_0\tau_m/\ln 2)]^{1/2})$ with $E_k = 1/2\mu_0 M_s V H'_{an}$, f_0 is the attempted frequency of the order of 1 GHz, and τ_m is the time measurement of the order of 1 s. By solving this equation using experimental parameters and assuming $f_0=1$ GHz, one finds $H'_{an} \approx 145$ Oe.
[48] B. Montigny and J. Miltat, J. Appl. Phys. **97**, 10C708 (2005).
[49] One can note, however, that the frequency derived from the m_x and the m_y components is the same for an out-of-plane precession mode.
[50] M. P. Sharrock, IEEE Trans. Magn. **26**, 193 (1990).